



Influence of Equation Nonlinearity on Pulse-Decay Permeability Measurements of Tight Porous Media

Yue Wang¹ · Zhiguo Tian¹ · Steffen Nolte² · Bernhard Krooss² · Moran Wang¹ 

Received: 28 September 2022 / Accepted: 7 April 2023
© The Author(s), under exclusive licence to Springer Nature B.V. 2023

Abstract

The pulse-decay method is believed to be more suitable than the steady-state method for permeability measurements on tight porous media because it records pressure variations instead of flow rates and does not require the establishment of a steady state. Most of the previous analytical solutions for the pulse-decay process are based on a linearized governing equation, which may be inapplicable to measurements with large differential pressures. In this study, a nonlinear governing equation is derived through mass conservation and Darcy's law. For rigid porous media such as the sedimentary rock samples, by comparing the magnitude of the pressure sensitivity of the physical properties for both the testing gas and the core sample, we found that only the gas compressibility and the apparent permeability have to be regarded as pressure-dependent, while the others can be regarded as constant. The perturbation method and the eigenfunction expansion method are combined to derive the general solution of the nonlinear governing equation. The results show that in the plot of logarithmic differential pressure versus time, a straight line can be obtained at the late-time stage and its slope value can be used to evaluate the apparent permeability. We further estimate the error in permeability evaluation, induced by selecting mean pore pressure as the characteristic pressure. The theoretical analysis has been verified by both numerical simulation and experimental measurements.

Keywords Pulse-decay method · Nonlinear · Pressure difference · Apparent permeability · Gas compressibility

List of Symbols

A	Cross-sectional area of cylindrical core sample, m^2
L	Length of cylindrical core sample, m
P	Pore pressure, Pa
P_D	Dimensionless pore pressure
$P_D^{(i)}$	The i th term in the asymptotic series
$P_D(\infty)$	Dimensionless equilibrium pore pressure

✉ Moran Wang
mrwang@tsinghua.edu.cn

¹ Department of Engineering Mechanics, Tsinghua University, Beijing 100084, China

² Institute of Geology and Geochemistry of Petroleum and Coal, Energy and Mineral Resources Group (EMR), RWTH Aachen University, Lochnerstr. 4-20, 52056 Aachen, Germany

P_c	Confining pressure, Pa
P_{char}	Characteristic pressure, Pa
$P_d(0)$	Initial downstream pressure, Pa
P_{eq}	Equilibrium pore pressure, Pa
P_{mean}	Mean pore pressure, Pa
$P_u(0)$	Initial upstream pressure, Pa
T	Temperature, K
V_u	Volume of upstream reservoir, m ³
V_d	Volume of downstream reservoir, m ³
Z	Gas compressibility factor
a	Volume ratio of sample's pore space to upstream reservoir
b	Volume ratio of sample's pore space to downstream reservoir
b_s	Klinkenberg slippage factor, Pa
f	Intercept in plot of dimensionless differential pressure versus time
k_{app}	Apparent permeability, m ²
k_{error}	Permeability coefficient evaluated with mean pore pressure as characteristic pressure, m ²
k_{int}	Intrinsic permeability, m ²
k_{real}	Permeability coefficient evaluated with equilibrium pore pressure as characteristic pressure, m ²
t	Time, s
t_D	Dimensionless time
v	Flow rate, m·s ⁻¹
w	Weight coefficient to determine characteristic pressure
x	Displacement, m
x_D	Dimensionless displacement
Γ	Dimensionless duration of a pulse-decay test
ΔP_D	Dimensionless differential pressure
α	Slope in plot of dimensionless differential pressure versus time
β_Z	Pressure sensitivity of gas compressibility factor, Pa ⁻¹
β_{b_s}	Pressure sensitivity of slippage factor, Pa ⁻¹
$\beta_{k_{app}}$	Pressure sensitivity of apparent permeability, Pa ⁻¹
$\beta_{k_{int}}$	Pressure sensitivity of intrinsic permeability, Pa ⁻¹
β_μ	Pressure sensitivity of viscosity, Pa ⁻¹
β_ρ	Gas compressibility, Pa ⁻¹
β_ϕ	Pressure sensitivity of porosity, Pa ⁻¹
δ	Relative error induced by misusing of characteristic pressure
ε	Strength of nonlinearity
θ_i	The i th positive solution to Eq. (37)
ρ	Gas density, kg·m ⁻³
μ	Dynamic viscosity of testing gas, Pa·s
ϕ	Porosity of core sample

1 Introduction

Permeability is one of the critical parameters for unconventional gas exploitation (Clarkson et al. 2012). Compared with conventional formations, unconventional formations are characterized by low matrix permeability coefficients, making permeability measurement

of unconventional rock samples a challenging task. The steady-state methods and the unsteady-state methods are the two major kinds of methods for measuring the permeability of rock samples in the laboratory (Sander et al. 2017; Lyu et al. 2020). For steady-state methods, the flow rate through the sample under a given pressure difference is monitored until steady-state conditions are reached. Then the permeability coefficient can be determined by Darcy's law with the pressure difference and steady-state flow rate (Boulin et al. 2012). The steady-state method is straightforward and does not require the estimation of storage terms. For unsteady-state methods, a steady state is not required, and the pressure transients are measured instead of the flow rates. For measurements on tight rocks, the unsteady-state methods are believed to be more suitable than the steady-state methods because establishing a steady state is usually time-consuming, and pressure is easier to measure and record compared to the flow rate (Chenevert and Sharma 1993; Akkutlu and Fathi 2012; Heller et al. 2014).

The pulse-decay method is one of the most widely used unsteady-state methods (Rushing et al. 2004; Alnoaimi and Kovscek 2019). In the original pulse-decay method pioneered by Brace et al. (1968), the sample was placed into a core holder and a gas reservoir of finite volume was connected to each end of the sample. The sample and the two reservoirs were first filled to the same initial pressure, and then the pressure in one reservoir was increased to create a pressure difference. Driven by the pressure difference, the gas flows through the sample from the reservoir with higher pressure (defined as the "upstream") to the one with lower pressure (defined as the "downstream"). For permeability evaluation, the upstream and downstream pressure variations were recorded over time. Some modified pulse-decay methods with different experimental designs have also been developed in recent decades. Jones (1972) developed the pressure falloff method, which involves keeping the downstream pressure constant and using upstream decay for permeability. The pressure build-up technique was proposed by Metwally and Sondergeld (2011), in which a constant pressure is applied to the upstream and the downstream pressure increase is recorded. Lasseux et al. (2012) proposed the so-called "step decay" method to simultaneously characterize several petrophysical properties of core samples. Yang et al. (2015) reported a simplified experimental configuration with only one gas reservoir. Hannon (2016) presented a bi-directional pulse-decay method in which pressure pulses of different amplitudes are applied to both reservoirs simultaneously.

Unlike in the steady-state method, in which the permeability coefficient can be calculated directly using Darcy's law, the permeability coefficient for the pulse-decay method is obtained by fitting observed pressure transients to the behavior predicted by the analytical solutions. By combining the law of conservation of mass with Darcy's law, Brace et al. (1968) derived the governing equation for gas transport in the pulse-decay process and simplified it into a linear form by limiting the relative pressure difference across the sample to less than 10%. They also obtained an approximate analytical solution (usually denoted as Brace et al.'s solution) for the pressure difference evolution, which is only valid when the reservoir volumes are much larger than the sample's pore volume. Lin (1977) and Trimmer (1981) discussed the possible errors in Brace et al.'s solution. Based on the same linear governing equation from Brace et al., Hsieh et al. (1981) and Dicker and Smits (1988) used the Laplace transform to obtain a general series solution (usually denoted as Dicker and Smits's solution) without restriction on the reservoir size.

Although Brace et al.'s and Dicker and Smits's solutions have been widely used, they are both based on the linearized governing equation, which ignores the influence of nonlinear factors and requires a small initial differential pressure. However, as reported in the literature (Walder and Nur 1986; Tinni et al. 2012; Wang et al. 2015; Ma et al.

2016; Hatami et al. 2022), many pulse-decay measurements have been performed with large pressure differences, in which the nonlinearity in the governing equations cannot be ignored and, thus, the applicability of the above linear solutions becomes questionable. Haskett et al. (1988) and Abdelmalek et al. (2018) suggested using pseudo-time and pseudo-pressure transformations to deal with the nonlinearities of the pulse-decay process, but the transformed governing equation is still nonlinear, and its analytical solution is missing. There also have been several approximate solutions considering the nonlinearity induced by gas compressibility changes during the pulse-decay process (Liang et al. 2001; Pan et al. 2015; Liu et al. 2017). Similar to Brace et al.'s solution, these approximate solutions are inapplicable for measurements with reservoir volumes comparable to or smaller than the pore volume.

In this study, we revisit the general governing equation of the pulse-decay process, taking into account the pressure dependence of the physical properties of both the testing gas (density, viscosity) and the core sample (permeability, porosity). The general equation is then simplified through the magnitude analysis of the nonlinear terms, and the perturbation method as well as the eigenfunction expansion method are used to analyze the behavior of the solution to the nonlinear problem. Numerical simulation and experimental measurements are performed to validate the theoretical results. The influence of nonlinearity on the test duration and the error in permeability evaluation, which is induced by improper selection of the characteristic pressure, are also discussed.

2 Mathematical Derivation

2.1 Governing Equation

The gas flow rate driven by a pressure gradient in porous media is determined by Darcy's law (Darcy 1856) as:

$$v = -\frac{k_{\text{app}}}{\mu} \frac{\partial P}{\partial x} \quad (1)$$

where v [$\text{m}\cdot\text{s}^{-1}$] is the flow rate, k_{app} [m^2] the apparent permeability coefficient, μ [$\text{Pa}\cdot\text{s}$] the dynamic viscosity of the testing gas, and P [Pa] is the gas pressure (also known as the pore pressure).

As shown in Fig. 1, for any position $x(0 \leq x \leq L)$ in the sample, the mass flux through the unit cross-sectional area is:

$$Q_x = \rho A v \quad (2)$$

where Q_x [$\text{kg}\cdot\text{s}^{-1}$] the mass flux, ρ [$\text{kg}\cdot\text{m}^{-3}$] the gas density, and A [m^2] the cross-sectional area. Then we consider a small volume between $x - \delta x/2$ and $x + \delta x/2$ within the sample. According to the law of conservation of mass, the difference between the inlet and outlet mass flow rates should be equal to the mass increase rate within the void fraction of the small volume:

$$\frac{\partial(\rho\phi)}{\partial t} + \frac{\partial}{\partial x}(\rho v) = 0 \quad (3)$$

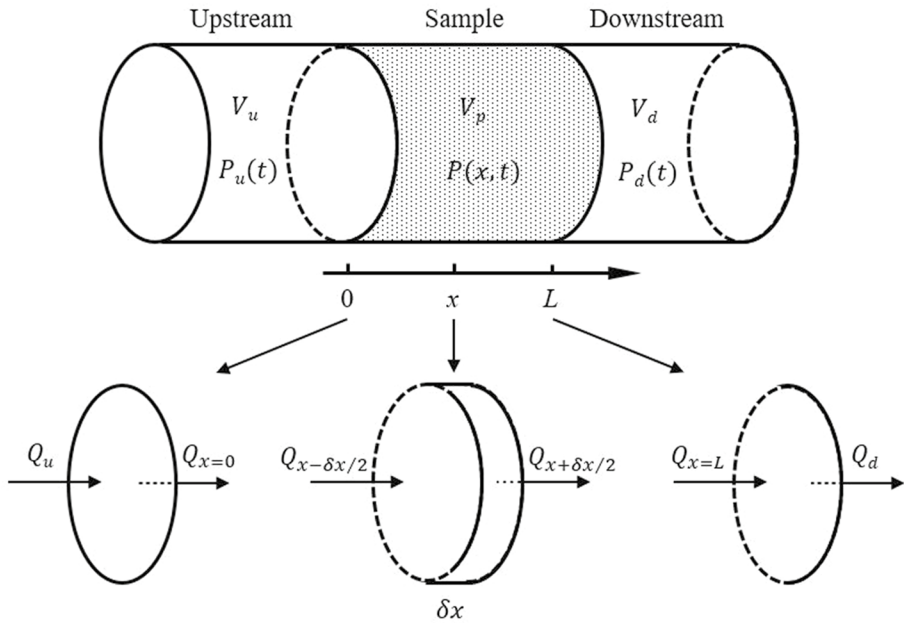


Fig. 1 Scheme of the pulse-decay test. The core sample is connected to two gas reservoirs at its two ends

where ϕ is the porosity of the sample.
 Substituting Eqs. (1) into (3) yields:

$$\frac{\partial(\rho\phi)}{\partial t} = \frac{\partial}{\partial x} \left(\rho \frac{k_{app}}{\mu} \frac{\partial P}{\partial x} \right) \tag{4}$$

It is noted that pore pressure P is the only parameter that can be measured directly in the pulse-decay test. Given the confining pressure P_c , the density ρ and viscosity μ of the gas, as well as the apparent permeability k_{app} and porosity ϕ of the sample, are all functions of the pore pressure. Equation (4) can be rewritten into a form with P as the independent variable:

$$\frac{\partial P}{\partial t} = \frac{k_{app}}{\mu\phi(\beta_\rho + \beta_\phi)} \left[\frac{\partial^2 P}{\partial x^2} + (\beta_\rho - \beta_\mu + \beta_{k_{app}}) \left(\frac{\partial P}{\partial x} \right)^2 \right] \tag{5}$$

where $\beta_X = \partial \ln X / \partial P$ ($X = \rho, \mu, k_{app}, \phi$) [Pa^{-1}] is the pressure sensitivity of X , which describes the relative change of X per unit pressure change. In literature (Brace et al. 1968), β_ρ is commonly referred to as the gas compressibility. It should be noted that the rock grain is assumed as rigid and non-reactive here. As a result, the grain compressibility and the fluid–solid pressure-stress coupling are both omitted. However, this assumption may not hold for highly stress-sensitive samples.

After obtaining the governing equation, the boundary conditions should also be derived. Since the flow resistance within the upstream and downstream reservoirs is much smaller

than that of the sample, the pressure within the reservoirs can be regarded as uniformly distributed. Taking the upstream side as an example, the mass flow out of the reservoir is:

$$Q_u = - \left. \frac{\partial(\rho V_u)}{\partial t} \right|_{x=0} \quad (6)$$

where V_u [m³] is the volume of the upstream reservoir. The mass flow into the sample can be calculate by lettering $x = 0$ in Eq. (2). According to the law of conservation of mass, at the interface between the upstream reservoir and the sample (see Fig. 1), the mass flow rate out of the upstream chamber and that into the sample should be equal:

$$\left. \frac{\partial(\rho V_u)}{\partial t} \right|_{x=0} = (\rho A v)|_{x=0} \quad (7)$$

Substituting Eqs. (1) into (7), and then rewriting the result with pressure as the independent variable yields:

$$\left. \frac{\partial P}{\partial t} \right|_{x=0} = \frac{k_{app} A}{(\beta_\rho + \beta_{V_u}) \mu V_u} \left. \frac{\partial P}{\partial x} \right|_{x=0} \quad (8)$$

Considering the interface between the downstream reservoir and the sample (see Fig. 1), the downstream boundary condition can also be derived:

$$\left. \frac{\partial P}{\partial t} \right|_{x=L} = - \frac{k_{app} A}{(\beta_\rho + \beta_{V_d}) \mu V_d} \left. \frac{\partial P}{\partial x} \right|_{x=L} \quad (9)$$

where V_d [m³] is the volume of the downstream reservoir, L [m] is the length of the sample. Unlike the conventional Dirichlet, Neumann, and Robin boundary conditions, Eqs. (8) and (9) involve both time and space derivatives. It is important to note that Eqs. (8) and (9) differ by a negative sign because in the upstream, the testing gas flows from the reservoir to the sample, while in the downstream the opposite is true.

Equations (5), (8) and (9) are the general governing equation and boundary conditions for the pulse-decay process, and only Darcy's law and the law of conservation of mass are used in their derivation. Despite the generality, obtaining an analytical solution to them is nearly impossible due to the strong nonlinearity. Numerical methods can be used to directly solve these general equations, and the resulting solutions can be fitted to the pressure data using the history matching method to determine the physical properties of the sample. However, the fitting algorithm must be carefully designed to prevent the occurrence of unphysical or non-unique results, particularly in multi-parameter fitting scenarios (Civan et al. 2012; Lin and Myers 2018). Therefore, the investigation of the analytical approximate solution is valuable as an alternative to the numerical solution, and it can also provide insights into the physical behavior of the pulse-decay process.

To facilitate the theoretical analysis, the pressure sensitivities appearing in Eqs. (5), (8) and (9) should be further analyzed. The dependence of gas density on pressure is described by the equation of state (Callen 1998):

$$\rho = \frac{M}{ZRT}P \tag{10}$$

where M [kg·mol⁻¹] is the molar mass of the gas, Z the compressibility factor, R [J·mol⁻¹·K⁻¹] the gas constant, and T [K] is the absolute temperature. Taking Eq. (10) into the definition of β_ρ , we have:

$$\beta_\rho = \frac{1}{P} - \left(\frac{\partial \ln Z}{\partial P} \right)_T = \beta_P - \beta_Z \tag{11}$$

where $1/P$ is denoted as β_P for consistency of notation.

The sample's apparent permeability is related to the gas pressure through the Klinkenberg formula (Klinkenberg 1941):

$$k_{app} = k_{int} \left(1 + \frac{b_s}{P} \right) \tag{12}$$

where k_{int} [m²] is the intrinsic permeability and b_s [Pa] is the slippage factor.

Substituting Eq. (12) into the definition of $\beta_{k_{app}}$, we have:

$$\beta_{k_{app}} = \beta_{k_{int}} + \frac{1}{P + b_s} - \frac{1}{P} + \frac{b_s}{P + b_s} \beta_{b_s} \tag{13}$$

Although the pressure sensitivities of the physical properties of the testing gas and the core sample all contribute to the nonlinearity of the governing equation, their magnitude is different, as shown in Table 1. The values of β_P , β_Z , and β_μ of the commonly used inert testing gases (He, Ar, N₂) in Table 1 are evaluated from the online dataset of NIST (Lemmon 2023) and those of $\beta_{k_{int}}$, β_{b_s} , and β_ϕ come from the literature on stress dependence of rock properties. Table 1 shows that the magnitudes of β_Z , β_μ , $\beta_{k_{int}}$, β_{b_s} , β_ϕ are much smaller than that of β_P , and thus can be safely omitted. In other words, Z , μ , k_{int} , b_s , and ϕ can all be treated as constants in a single measurement and their values are taken under a characteristic pressure P_{char} between $P_u(0)$ and $P_d(0)$. Only the gas compressibility and the apparent permeability are considered to be pressure-dependent. The value of grain compressibility β_m is also listed in Table 1, and it is much smaller than the value of β_P , which justifies our assumption of rigid grains during the derivation.

After the magnitude comparison, we have:

$$\beta_\rho \approx \beta_P = \frac{1}{P} \tag{14}$$

Table 1 Magnitude of the pressure sensitivities for physical properties of the gas and sample

Type	Variable	Magnitude (MPa ⁻¹)	Sources
Gas (He, Ar, N ₂)	β_P	10 ⁻¹ ~ 10 ¹	NIST online dataset Lemmon (2023)
	β_Z	10 ⁻³ ~ 10 ⁻²	(https://webbook.nist.gov/chemistry/fluid/)
	β_μ	10 ⁻³ ~ 10 ⁻²	
Sample (Sedimentary rock matrix)	$\beta_{k_{int}}$	10 ⁻³ ~ 10 ⁻²	Katsube (2000); Dong et al. (2010); Heller et al. (2014); Ghanizadeh et al. (2014a); Ghanizadeh et al. (2014b); Zhang et al. (2015); Letham and Bustin (2016); Pang et al. (2017); Fink et al. (2017); Davudov et al. (2018); Chen et al. (2019)
	β_{b_s}	10 ⁻³ ~ 10 ⁻²	
	β_ϕ	10 ⁻⁴ ~ 10 ⁻²	
	β_m	10 ⁻⁴ ~ 10 ⁻³	

$$\beta_{k_{app}} \approx \frac{1}{P + b_s} - \frac{1}{P} \tag{15}$$

With Eqs. (12), (14) and (15), Eq. (5) reduces to a much simplified but still nonlinear form:

$$\frac{\partial P}{\partial t} = \frac{k_{int}}{\mu\phi} \left[(P + b_s) \frac{\partial^2 P}{\partial x^2} + \left(\frac{\partial P}{\partial x} \right)^2 \right] = \frac{k_{int}}{\mu\phi} \frac{\partial}{\partial x} \left[(P + b_s) \frac{\partial P}{\partial x} \right] \tag{16}$$

Due to the consideration of the pressure dependence of gas compressibility and apparent permeability, Eq. (16) not only has the second-order spatial derivative of pore pressure but also an extra nonlinear term of the squared pressure gradient, while the governing equation in Brace et al. (1968) only has the former. Moreover, the coefficient before the second-order spatial derivative is no longer a constant, which further strengthens the nonlinearity of Eq. (16). Note that when the test gases are carbon dioxide and methane, approximating β_ρ to $1/P$ may no longer hold and the adsorption on the pore walls must also be considered (Cui et al. 2009).

It is noted that the reservoirs are generally made of stainless steel, whose compressibility is much smaller than that of the testing gas. Therefore, we have $\beta_{V_u}, \beta_{V_d} \ll \beta_\rho$, and V_u, V_d can be regarded as a constant. By substituting Eqs. (12) and (14) into Eqs. (8) and (9), the simplified boundary conditions at the interfaces between the gas reservoirs and the two ends of the sample can be obtained as:

$$\left. \frac{\partial P}{\partial t} \right|_{x=0} = \frac{k_{int}A}{\mu V_u} (P + b_s) \left. \frac{\partial P}{\partial x} \right|_{x=0} \tag{17}$$

$$\left. \frac{\partial P}{\partial t} \right|_{x=L} = -\frac{k_{int}A}{\mu V_d} (P + b_s) \left. \frac{\partial P}{\partial x} \right|_{x=L} \tag{18}$$

In the pulse-decay test initiated by applying a positive pressure pulse to the upstream reservoir, the initial condition is given by:

$$P(x, 0) = \begin{cases} P_u(0), & x = 0 \\ P_d(0), & 0 < x \leq L \end{cases} \tag{19}$$

Here $P_u(0)$ and $P_d(0)$ [Pa] are the upstream and downstream pressures immediately after the application of the pressure pulse, respectively.

The above equations are all in a dimensional form. For ease of analysis, the following dimensionless variables are introduced:

$$x_D = \frac{x}{L}, t_D = \frac{(P_{char} + b_s)k_{int}t}{\mu\phi L^2}, P_D = \frac{P - P_d(0)}{P_u(0) - P_d(0)}, a = \frac{LA\phi}{V_u}, b = \frac{LA\phi}{V_d} \tag{20}$$

where x_D, t_D, P_D are the dimensionless counterparts of x, t, P , respectively, and a, b are the volume ratios of the sample's pore space to the upstream and downstream reservoir, respectively. The characteristic pressure P_{char} [Pa] is defined as the weighted average of the initial upstream and downstream pressures:

$$P_{char} = wP_u(0) + (1 - w)P_d(0) \tag{21}$$

where w is the weighting coefficient to be determined.

With these dimensionless variables, the governing Eq. (16) can be rewritten in a dimensionless form:

$$\frac{\partial P_D}{\partial t_D} = \frac{\partial^2 P_D}{\partial x_D^2} + \varepsilon \frac{\partial^2}{\partial x_D^2} (P_D - w)^2 \tag{22}$$

and the dimensionless boundary and initial conditions are:

$$\left. \frac{\partial P_D}{\partial t_D} \right|_{x_D=0} = a \left. \frac{\partial P_D}{\partial x_D} \right|_{x_D=0} + \varepsilon a \left. \frac{\partial}{\partial x_D} (P_D - w)^2 \right|_{x_D=0} \tag{23}$$

$$\left. \frac{\partial P_D}{\partial t_D} \right|_{x_D=1} = -b \left. \frac{\partial P_D}{\partial x_D} \right|_{x_D=1} - \varepsilon b \left. \frac{\partial}{\partial x_D} (P_D - w)^2 \right|_{x_D=1} \tag{24}$$

$$P_D(x_D, 0) = \begin{cases} 1, & x_D = 0 \\ 0, & 0 < x_D \leq 1 \end{cases} \tag{25}$$

where ε is a dimensionless parameter defined as:

$$\varepsilon = \frac{1}{2} \frac{P_u(0) - P_d(0)}{P_{char} + b_s} \tag{26}$$

Compared with the linear equations by Brace et al. (1968), Eqs. (22)–(24) contain additional nonlinear terms, the strength of which is quantified by ε . According to the definition, ε is proportional to the initial pressure difference and is inversely related to the characteristic pressure and slippage factor. Since the relative initial pressure difference rarely exceeds 100% and the slippage factor can be in the order of MPa (Ghanizadeh et al. 2014a, 2014b; Letham and Bustin 2016; Chen et al. 2019), the value of ε is generally in the range of 0–0.5. If $\varepsilon = 0$, the nonlinear terms in Eqs. (22)–(24) vanish and the equations reduce to the linear form proposed by Brace et al. (1968). However, this only holds when the initial pressure difference across the sample is infinitely small. In practice, the initial pressure difference is not negligible, the influence of the nonlinear terms must be carefully evaluated.

2.2 The asymptotic Solution

It is usually very difficult, or even impossible, to obtain the general analytical solution to a nonlinear problem. The perturbation method is adopted in this section to obtain the asymptotic solution. The idea behind the perturbation theory (Bender and Orszag 2013) is to divide the original problem into two parts: linear and perturbative. The solution to the original problem is expressed as a power series with a small perturbative parameter. The first term of the series solution is the exact solution to the linear part, and the successive terms correspond to the perturbative part. The series solution is also called an asymptotic solution (Hinch 1991).

To solve the nonlinear equations above, we choose ε as the perturbative parameter, and then expand the solution into a series of ε :

$$P_D(x_D, t_D) = \varepsilon^0 P_D^{(0)}(x_D, t_D) + \varepsilon^1 P_D^{(1)}(x_D, t_D) + \varepsilon^2 P_D^{(2)}(x_D, t_D) + \dots \tag{27}$$

As shown in Eq. (26), the perturbative parameter ε depends on the characteristic pressure P_{char} that is subject to change with the weighting coefficient w . Although the solution $P_D(x_D, t_D)$ is unique, by altering w , it can be expanded into a series with different forms. We will show that a certain value of w is superior to the others since it can help to expand the solution into a simple form.

The governing equation, as well as the boundary and initial conditions for $P_D^{(i)}$, can be obtained by substituting Eq. (27) into Eqs. (22)–(24). For brevity, only the equations for $P_D^{(0)}$ and $P_D^{(1)}$ are listed below.

For $P_D^{(0)}$, the governing equation is:

$$\frac{\partial P_D^{(0)}}{\partial t_D} = \frac{\partial^2 P_D^{(0)}}{\partial x_D^2} \tag{28}$$

and the boundary and initial conditions are:

$$\left. \frac{\partial P_D^{(0)}}{\partial t_D} \right|_{x_D=0} = a \left. \frac{\partial P_D^{(0)}}{\partial x_D} \right|_{x_D=0} \tag{29}$$

$$\left. \frac{\partial P_D^{(0)}}{\partial t_D} \right|_{x_D=1} = -b \left. \frac{\partial P_D^{(0)}}{\partial x_D} \right|_{x_D=1} \tag{30}$$

$$P_D^{(0)}(x_D, 0) = \begin{cases} 1, & x_D = 0 \\ 0, & 0 < x_D \leq 1 \end{cases} \tag{31}$$

The governing equation for $P_D^{(1)}$ is:

$$\frac{\partial P_D^{(1)}}{\partial t_D} = \frac{\partial^2 P_D^{(1)}}{\partial x_D^2} + \frac{\partial^2}{\partial x_D^2} (P_D^{(0)} - w)^2 \tag{32}$$

and the boundary and initial conditions are:

$$\left. \frac{\partial P_D^{(1)}}{\partial t_D} \right|_{x_D=0} = a \left. \frac{\partial P_D^{(1)}}{\partial x_D} \right|_{x_D=0} + a \left. \frac{\partial}{\partial x_D} (P_D^{(0)} - w)^2 \right|_{x_D=0} \tag{33}$$

$$\left. \frac{\partial P_D^{(1)}}{\partial t_D} \right|_{x_D=1} = -b \left. \frac{\partial P_D^{(1)}}{\partial x_D} \right|_{x_D=1} - b \left. \frac{\partial}{\partial x_D} (P_D^{(0)} - w)^2 \right|_{x_D=1} \tag{34}$$

$$P_D^{(1)}(x_D, 0) = \begin{cases} 0, & x_D = 0 \\ 0, & 0 < x_D \leq 1 \end{cases} \tag{35}$$

It is important to note that while the governing equation and boundary conditions of $P_D^{(0)}$ are homogeneous, while those of $P_D^{(1)}$ contain inhomogeneous terms. This is a direct result of the ϵ -dependent nonlinear terms present in Eqs. (22)–(24). After the perturbative expansion to the power series of ϵ , these nonlinear terms start at from ϵ^1 rather than ϵ^0 , resulting in homogeneous governing equation and boundary conditions for $P_D^{(0)}$, and inhomogeneous ones for $P_D^{(i)}$ ($i \geq 1$).

Equations (28)–(31) for $P_D^{(0)}$ are actually the linear problem solved by Dicker and Smits (1988), so $P_D^{(0)}$ is just the Dicker and Smits’s solution:

$$P_D^{(0)}(x_D, t_D) = P_D(\infty) + \sum_{m=1}^{\infty} f_m(x_D) e^{-\theta_m^2 t_D} \tag{36}$$

where $P_D(\infty) = b/(a + b + ab)$ is the dimensionless equilibrium pore pressure, θ_m ($m \geq 1$) the m th positive solution of the following equation:

$$\tan \theta_m = \frac{(a + b)\theta_m}{\theta_m^2 - ab} \tag{37}$$

and $f_m(x_D)$ ($m \geq 1$) is given by

$$f_m(x_D) = \frac{2(\theta_m^2 - ab) [\theta_m \sin(\theta_m - \theta_m x_D) - b \cos(\theta_m - \theta_m x_D)]}{[\theta_m^4 + (a^2 + b^2 + a + b)\theta_m^2 + ab(ab + a + b)] \cos(\theta_m)} \tag{38}$$

Although the full expression for $P_D^{(0)}$ in Eq. (36) is composed of a series of exponentials, as time increases, most exponential terms will become negligible, leaving only the first term as $0 < \theta_1 < \theta_2 < \dots$. Therefore, we have:

$$P_D^{(0)}(x_D, t_D) \approx P_D(\infty) + f_1(x_D) e^{-\theta_1^2 t_D} \tag{39}$$

which is referred to as the late-time solution in the literature (Bhandari et al. 2015; Sander et al. 2017) and it indicates that $P_D^{(0)}$ across the system decays toward the equilibrium pore pressure exponentially. The late-time stage of a pulse-decay test is defined as the stage where the complete series solution can be well approximated by the late-time solution of a single exponent.

Because of the extra terms containing $(P_D^{(0)} - w)^2$, Eqs. (32)–(34) for $P_D^{(1)}$ are inhomogeneous. The eigenfunction expansion method (Riley et al. 1999; Loney 2006) is adopted here to solve $P_D^{(1)}$. Once $P_D^{(0)}$ is known, $P_D^{(2)}$ and the higher order terms can be sequentially solved. The derivation process is standard but somewhat tedious, and therefore, omitted here. The focus is instead on the analysis the analytical solutions’ characteristics. According to Eq. (36), $(P_D^{(0)} - w)^2$ contains an infinite number of exponential terms with different exponents, and so is the expression of $P_D^{(1)}$. At the early-time stage of the pulse decay process, these exponential terms of the same magnitude, so the expression of $P_D^{(1)}$ cannot be simplified by omitting any of them. The complex form of the series makes it difficult to use. However, at the late-time stage of the pulse-decay process, the terms with large exponents become insignificant, and $P_D^{(1)}$ can be well approximated by the term with the smallest exponents. Similar analysis holds for $P_D^{(i)}$ ($i \geq 2$). Therefore, at the late-time stage of the pulse-decay process, we have:

$$P_D^{(i)}(x_D, t_D) = \begin{cases} \mathcal{O}\left(e^{-\theta_1^2 t_D}\right), & w = P_D(\infty), i \geq 1 \\ \mathcal{O}\left(t_D^i e^{-\theta_1^2 t_D}\right), & w \neq P_D(\infty), i \geq 1 \end{cases} \tag{40}$$

where the \mathcal{O} notation is used to describe the diminishing order of $P_D^{(i)}$ when time tends to infinity. Equation (40) indicates that if we set $w = P_D(\infty)$, $P_D^{(i)}$ ($i \geq 1$) will decay with the exponent $-\theta_1^2$ at the late-time stage, as does $P_D^{(0)}$. However, when we set $w \neq P_D(\infty)$, $P_D^{(i)}$ ($i \geq 1$) will not be reduced to a single exponential form.

Recalling the asymptotic series from Eq. (27), the late-time behavior of P_D can be obtained by superimposing $P_D^{(i)}$ ($i \geq 0$) times the corresponding power of ϵ . When $w = P_D(\infty)$, we have:

$$P_D(x_D, t_D) = P_D^{(0)} + \epsilon P_D^{(1)} + \epsilon^2 P_D^{(2)} + \dots = P_D(\infty) + \mathcal{O}\left(e^{-\theta_1^2 t_D}\right), w = P_D(\infty) \tag{41}$$

Although the detailed expression for the coefficient of the exponential term are complex, Eq. (41) shows that with a proper choice of w , the solution P_D to the nonlinear problem (22)–(25) will exhibit exponential decay to its equilibrium value in the late-time stage of the pulse-decay test, like the solution $P_D^{(0)}$ obtained from the linear problem (28)–(31). As all terms in the perturbative solution have been added together, Eq. (41) holds over a large range of ϵ values.

In the pulse-decay measurements, the pressure transients at both ends of the sample are monitored over time, and the difference between them is used for permeability evaluation. By letting $x_D = 0$ and $x_D = 1$ in Eq. (36) and then taking the difference, we have:

$$\Delta P_D^{(0)}(t_D) = P_D^{(0)}(0, t_D) - P_D^{(0)}(1, t_D) = \mathcal{O}\left(e^{-\theta_1^2 t_D}\right) \tag{42}$$

The late-time characteristic of high order terms for differential pressure can be obtained from Eq. (40) in a similar manner:

$$\Delta P_D^{(i)}(t_D) = P_D^{(i)}(0, t_D) - P_D^{(i)}(1, t_D) = \begin{cases} \mathcal{O}\left(e^{-\theta_1^2 t_D}\right), & w = P_D(\infty) \\ \mathcal{O}\left(t_D^i e^{-\theta_1^2 t_D}\right), & w \neq P_D(\infty) \end{cases} \tag{43}$$

Combining Eqs. (42) and (43), we have:

$$\Delta P_D(t_D) = \sum_{i=0}^{\infty} \epsilon^i \Delta P_D^{(i)}(0, t_D) = \mathcal{O}\left(e^{-\theta_1^2 t_D}\right), w = P_D(\infty) \tag{44}$$

which shows that when the nonlinear effects are considered, the dimensionless differential pressure still reduces to a single exponential form at the late-time stage of the pulse-decay test with $w = P_D(\infty)$. However, if the other value of w is chosen, the corresponding expression for ΔP_D remains in the form of a series at the late-time stage, making it difficult to determine the decay characteristic of ΔP_D .

By inserting $w = P_D(\infty)$ in Eq. (21), we have:

$$P_{\text{char}} = P_D(\infty)[P_u(0) - P_d(0)] + P_d(0) = P_{\text{eq}} \tag{45}$$

In other words, $w = P_D(\infty)$ means choosing equilibrium pore pressure P_{eq} as the characteristic pressure. Substituting Eqs. (45) into (44) and converting the dimensionless time to its dimensional form with Eq. (20) yields:

$$\Delta P_D(t_D) = \mathcal{O}\left(\exp\left(-\frac{k_{\text{int}}(P_{\text{eq}} + b_s)\theta_1^2 t}{\mu\phi L^2}\right)\right) \tag{46}$$

Taking the logarithm of Eq. (46), we have:

$$\ln \Delta P_D(t) \approx f + \alpha t \tag{47}$$

where the “ \approx ” here indicates that the equality holds only in the late-time stage, f is a constant that depends on a , b and ε . The expression of α is:

$$\alpha = -\frac{k_{\text{int}}(P_{\text{eq}} + b_s)\theta_1^2}{\mu\phi L^2} \tag{48}$$

Equation (47) shows that in the plot of the dimensionless differential pressure $\ln \Delta P_D$ versus time t , a straight line with slope α and intercept f can be obtained at the late-time stage. In practice, the values of α and f can be determined by a linear fit of the experimental pressure data, and the measurement can be stopped after entering the late-time stage and enough data have been collected without reaching final equilibrium.

By transforming Eq. (48), we have:

$$k_{\text{app}}(P_{\text{eq}}) = k_{\text{int}}\left(1 + \frac{b_s}{P_{\text{eq}}}\right) = -\frac{\alpha\beta_\rho\mu\phi L^2}{\theta_1^2} \tag{49}$$

where $\beta_\rho = 1/P_{\text{eq}}$ is the gas compressibility at the equilibrium pore pressure P_{eq} . Equation (49) shows that the value of slope α can be used to obtain the apparent permeability $k_{\text{app}}(P_{\text{eq}})$ when the gas compressibility at P_{eq} is taken into account. Such a way of using α as an intermediate variable for permeability calculation was first proposed by Brace et al. (1968) based on the theoretical analysis of the linear governing equation. It should be noted the analysis in the present study is based on the nonlinear governing equation, and therefore Eq. (49) is applicable for measurements with a large initial pressure difference.

There are several methods to determine the equilibrium pressure in a pulse-decay test. The direct one is to wait for the pressure difference to vanish and the system to reach equilibrium, which is time-consuming and decreases measurement efficiency. An alternative way involves using the law of conservation of mass to calculate the equilibrium pressure based on the initial upstream and downstream pressures. However, this method requires prior knowledge of the sample’s pore volume. Wang et al. (2022) have developed expressions for the equilibrium pressure with only the upstream and downstream pressure transients as input. These expressions can give equilibrium pressure values as soon as the system reaches the late-time stage and do not require the pore volume of the sample.

3 Numerical Simulation

As shown above, the perturbation method and the eigenfunction expansion method helped to give the late-time behavior of the pressure transients, but they are inapplicable to analyzing the pressure variation at the other stages. The numerical simulation was performed to further investigate the influence of nonlinearity. The finite difference method is adopted in the numerical simulation. The governing equation, together with the boundary and initial conditions, was discretized by the Crank-Nicolson scheme (Crank and Nicolson 1947) that has second-order accuracy in both time and space, and the nonlinear terms were coped with by Richtmyer’s linearization method (Richtmyer and Morton 1994).

First, the late-time behavior of $\Delta P_D^{(i)}$ ($i = 0, 1, 2$) is solved numerically to verify the theoretical results in the previous section. The simulated $\ln \Delta P_D^{(0)}$ with $a = b = 1$ is presented in Fig. 2a, where a linear decline is found as time proceeds, which is consistent with its analytical form in Eq. (42). Figure 2b and c compares $\Delta P_D^{(1)}$ and $\Delta P_D^{(2)}$ with $\Delta P_D^{(0)}$ for different values of w , and the results show that when $w = P_D(\infty)$, the ratios of $\Delta P_D^{(1)}$ and $\Delta P_D^{(2)}$ to $\Delta P_D^{(0)}$ finally converge to constants, indicating that at the late-time stage $\Delta P_D^{(1)}$ and $\Delta P_D^{(2)}$ decay at the same rate as $\Delta P_D^{(0)}$. However, when $w \neq P_D(\infty)$, the ratios of $\Delta P_D^{(1)}$ and $\Delta P_D^{(2)}$

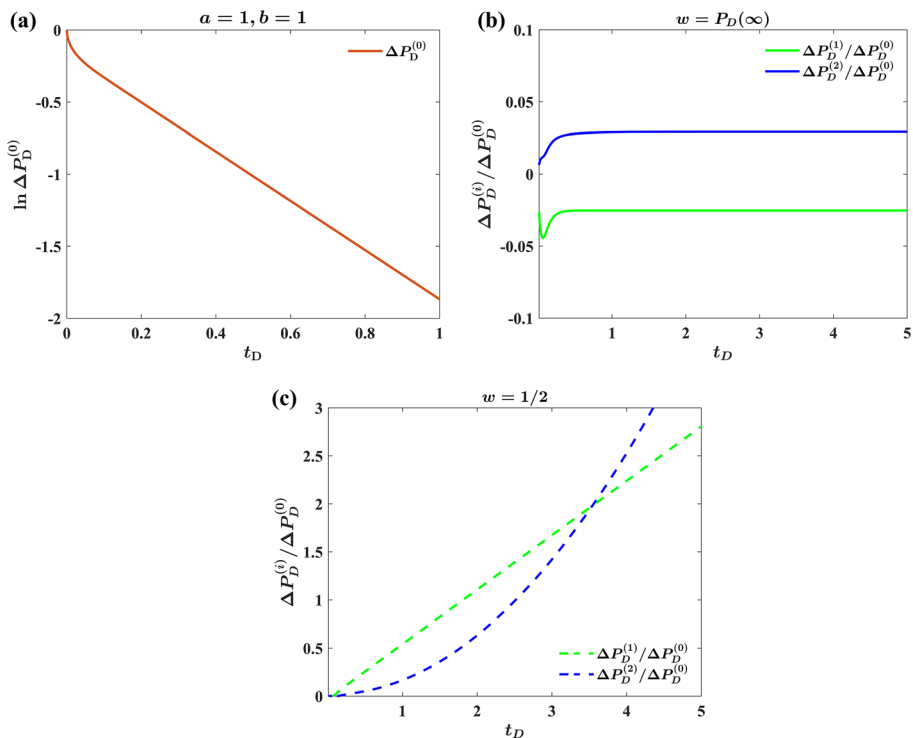


Fig. 2 Numerical simulation of $P_D^{(0)}$, $P_D^{(1)}$ and $P_D^{(2)}$. Here we set $a = b = 1$ and therefore $P_D(\infty) = 1/3$. **a** The variations of $\ln \Delta P_D^{(0)}$, **b** the variations $\Delta P_D^{(1)}/\Delta P_D^{(0)}$ and $\Delta P_D^{(2)}/\Delta P_D^{(0)}$ with $w = P_D(\infty)$, **c** the variations $\Delta P_D^{(1)}/\Delta P_D^{(0)}$ and $\Delta P_D^{(2)}/\Delta P_D^{(0)}$ with $w = 1/2$

to $\Delta P_D^{(0)}$ exhibit linear and quadratic growth over time, respectively. The numerical results given in Fig. 2 are in full agreement with the theoretical prediction in Eq. (43).

By finite difference simulation of Eqs. (22)–(25), the numerical solution of P_D is obtained to validate the perturbative solution. As shown in Eq. (27), the perturbative solution is in the form of a power series of perturbation parameter ϵ . when ϵ is small, using the first-order term in the power series can approximate the full series very well. However, when the parameter is large, more terms must be added to improve accuracy. Figure 3 gives the comparison between the perturbative solution and the numerical solution of P_D for $\epsilon = 0.5$, and the results show that perturbative solution retaining the first four terms agrees well with the numerical solution, and the relative error δ between them is less than 1%.

By numerically solving Eqs. (22)–(25), where $w = P_D(\infty)$ and changing the value of ϵ to modify the strength of nonlinearity, the variations of P_D are obtained. $\epsilon = 0$ denotes the linear case where nonlinear effects can be ignored (i.e., the Dicker and Smits’s solution), and it can be achieved by applying an infinitely small initial pressure difference in the pulse-decay test. The cases with $\epsilon > 0$ can be understood as the tests performed for the same sample under finite pressure differences but the same equilibrium pore pressure.

Figure 4a shows the up- and downstream pressure transients when the sample is connected to two gas reservoirs of the same volume as its pore space ($a = 1, b = 1$). Driven by the pressure difference, the gas flows from upstream to downstream, causing the upstream pressure to fall and the downstream pressure to rise. Finally, the pressure difference is eliminated and the whole system reaches equilibrium. In the linear case, the physical properties of the testing gas and core sample are all treated as constants, and their values are taken under the equilibrium pore pressure. In the nonlinear case, the values of the gas compressibility and apparent permeability are determined by the local transient pressure, making the pressure change rate proportional to the pressure itself, as seen in Eqs. (17) and (18). Note that the equilibrium pore pressure is less than the upstream but greater than the downstream pressure, so that the upstream pressure in the nonlinear case ($\epsilon > 0$) decreases faster and the downstream pressure rises more slowly than in the linear case ($\epsilon = 0$). However, when considering the pressure difference, the nonlinear effects in the upstream and downstream compartments largely cancel out, resulting in the logarithmic pressure difference

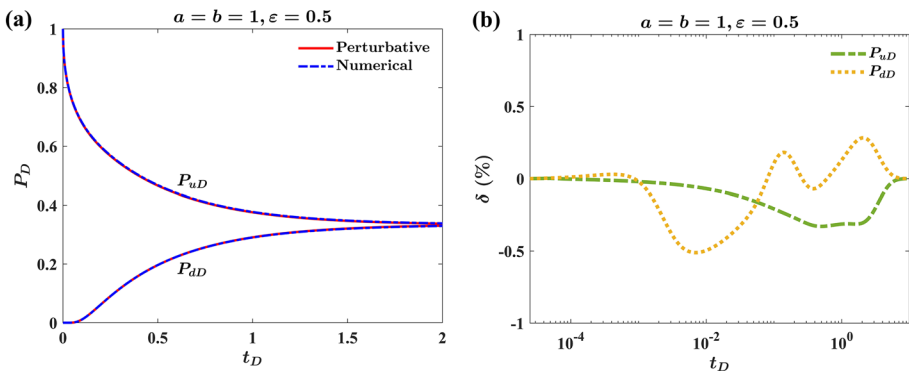


Fig. 3 Comparison between the perturbative and numerical solutions. **a** Variations of the upstream and downstream pressure with $a = b = 1, \epsilon = 0.5$ **b** Relative error between the perturbative and numerical solutions

curves with different values of ε in Fig. 3b nearly overlapping. As time proceeds, these curves decline linearly with the same slope, which is consistent with Eq. (47) in Sect. 2.

The pressure falloff case, in which a reservoir of finite volume is connected to the upstream and a constant pressure is maintained in the downstream compartment ($a = 1, b = 0$), is shown in Fig. 4c and d. Due to the nonlinear effect, the upstream pressure drops faster with $\varepsilon > 0$ than with $\varepsilon = 0$. However, since the downstream reservoir is “infinitely large”, the downstream pressure always remains at its initial value irrespective of the amount of gas that is transferred into the downstream from the upstream compartment. As a result, the nonlinear effects on the upstream cannot be offset by the downstream and it can be seen from Fig. 4d that the logarithmic differential pressures with different values of ε no longer overlap, but become parallel at the late-time stage. With larger ε , the logarithmic differential pressure will have a more “negative” intercept. Figure 4e and f depicts the pressure build-up case, in which a constant pressure is applied upstream of the sample and a finite-volume reservoir is connected downstream ($a = 0, b = 1$). The downstream pressure increase is slowed down by the nonlinearity, making the intercept of the logarithmic differential pressure more “positive”.

4 Experimental Measurements

Experimental measurements were performed to verify the theoretical and numerical results presented in the previous sections. The setup used in the measurement is described in detail in our previous researches (Gaus et al. 2019; Nolte et al. 2021), and the other parameters are summarized in Table 2. Helium is chosen as the testing gas to minimize the effect of adsorption. The grey Weser sandstone sample tested in this study originates from the Trendelburg beds of the Reinhardswald Basin in Germany. The sample was dried under vacuum at 105 °C until its weight became constant.

In the measurements, the upstream side of the sample is connected to two gas reservoirs of finite volume. The whole system, including the core sample, is initially saturated with helium and equilibrated at the desired pressure level (≈ 2.3 bar). The downstream reservoir is then directly open to the atmosphere to create the initial pressure difference. As the gas flows from upstream through the sample to the downstream side, the upstream pressure decreases until it finally equals the atmospheric pressure, also the equilibrium pore pressure, and the downstream pressure remains constant during the measurements. Four measurement was performed to ensure repeatability.

Table 2 Parameters of pulse-decay measurements

Parameter	Value
Confining pressure P_c (bar)	200
Equilibrium pore pressure P_{eq} (atm)	1
Temperature T (°C)	35
Gas viscosity μ (Pa·s)	2.07×10^{-5}
Sample porosity ϕ (%)	8.79
Sample length L (m)	68×10^{-3}
Sample diameter D (m)	38×10^{-3}

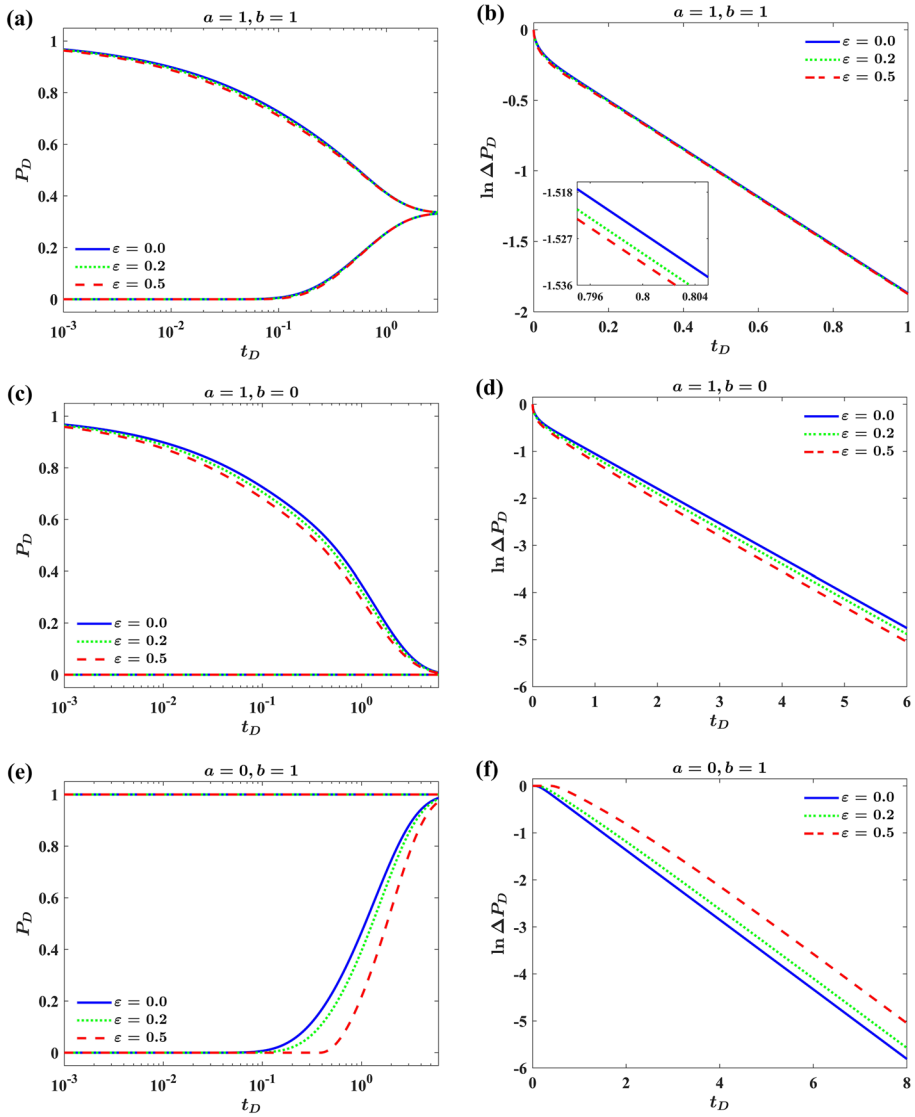


Fig. 4 Numerical simulation of variations of P_D and $\ln \Delta P_D$ over t_D with $w = P_D(\infty)$. $\epsilon = 0$ denotes the linear solution (i.e., Dicker and Smits' solution), and $\epsilon > 0$ denotes the nonlinear solution. **a** Variations of P_{uD} and P_{dD} with $a = b = 1$, **b** variations of $\ln \Delta P_D$ with $a = b = 1$, **c** variations of P_{uD} and P_{dD} with $a = 1, b = 0$, **d** variations of $\ln \Delta P_D$ with $a = 1, b = 0$, **e** variations of P_{uD} and P_{dD} with $a = 0, b = 1$, **f** variations of $\ln \Delta P_D$ with $a = 0, b = 1$

To verify the importance of nonlinearity in pulse-decay measurements with large differential pressure, the linear and the nonlinear (perturbative) solutions are compared with the experimental data, and the results are shown in Fig. 5. In the linear solution ($\epsilon = 0$), the gas compressibility and apparent permeability are considered constant, while in the nonlinear solution ($\epsilon = 0.1$), the gas compressibility and apparent permeability are both pressure-dependent.

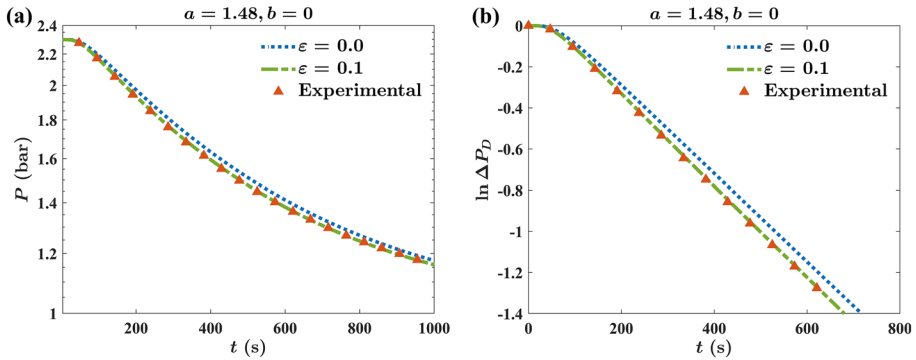


Fig. 5 Pulse-decay measurements on a grey Weser sandstone sample. The red triangles denotes the experimental results, and the dashed blue line and the green dotted line represents the results of the linear and nonlinear (perturbative) solutions, respectively. **a** The upstream pressures against time **b** the logarithm of dimensionless differential pressure against time

Figure 5a presents the upstream pressure transients of the pulse-decay process on the grey Weser sandstone sample. As gas depletion occurs, the upstream reservoir pressure decreases with time. The experimental upstream pressure deviates from the linear solution but agrees well with the nonlinear solution. This is because the linear solution ignores the pressure dependence of the gas compressibility and apparent permeability and takes their values under the equilibrium pressure. In the experimental measurements, the upstream pressure is always higher than the equilibrium pressure, so according to Eq. (17), the actual upstream pressure drops faster than that predicted by the linear solution. The agreement between the experimental data and the nonlinear solution indicates the importance of nonlinearity and the inadequacy of linear governing equations.

The logarithm of the dimensionless differential pressure is presented against time in Fig. 5b. As predicted by the theoretical analysis, both the linear and nonlinear solutions converge to straight lines shortly after the start of the test. Although the curves are parallel in the late-time stage, they exhibit different intercepts. The nonlinear solution closely matches the experimental data, while the linear solution deviates from it. The results shown in Fig. 5 are consistent with the theoretical analysis in Sect. 2 (see Eqs. (47) and (48)) and the numerical simulation in Sect. 3 (see Fig. 4c and d). These results provide evidence that the proposed nonlinear governing equation accurately captures the effect of nonlinearity in the pulse-decay process.

5 Discussion

5.1 The permeability Evaluation Error Induced by Setting $P_{\text{char}} = P_{\text{mean}}$

It is proved in Sect. 2 that the logarithmic differential pressure decays linearly with time at the late-time stage of the pulse-decay test. The slope (or decay rate) can be used to evaluate apparent permeability when the equilibrium pore pressure is selected as the characteristic pressure. That is, by substituting the gas compressibility and viscosity under the equilibrium pore pressure into Eq. (47), the apparent permeability under the equilibrium pore pressure can be obtained. In some previous studies (Jones 1997; Metwally and Sondergeld 2011; Bhandari

et al. 2015; Yang et al. 2015; Lin and Myers 2018), the mean pore pressure P_{mean} was taken as the characteristic pressure:

$$P_{\text{mean}} = \frac{1}{2}P_u(0) + \frac{1}{2}P_d(0) \tag{50}$$

In general, the equilibrium pore pressure is not equal to the mean pore pressure. In the pulse-decay tests where the initial pulse is generated by pressurizing the upstream reservoir, the dimensionless equilibrium pore pressure is $b/(a + b + ab)$, which is generally not equal to 1/2, even when the upstream and downstream reservoirs are of the same volume ($a = b$). In pressure build-up and pressure falloff tests, the equilibrium pore pressure equals $P_u(0)$ and $P_d(0)$, respectively, rather than P_{mean} . By replacing P_{eq} on the left side of Eq. (48) with P_{mean} , we find that the result is not the apparent permeability under the mean pore pressure, so we denote it as k_{error} :

$$k_{\text{error}} = k_{\text{int}} \left(\frac{P_{\text{eq}}}{P_{\text{mean}}} + \frac{b_s}{P_{\text{mean}}} \right) = -\frac{\alpha \mu \phi L^2}{P_{\text{mean}} \theta_1^2} \tag{51}$$

The “real” apparent permeability under the mean pore pressure is denoted as k_{real} :

$$k_{\text{real}} = k_{\text{app}}(P_{\text{mean}}) = k_{\text{int}} \left(1 + \frac{b_s}{P_{\text{mean}}} \right) \tag{52}$$

and the error in the permeability evaluation, induced by selecting mean pore pressure as characteristic pressure, is defined as:

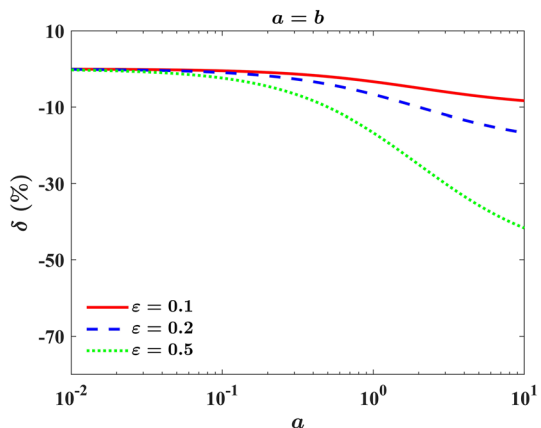
$$\delta = \frac{k_{\text{error}} - k_{\text{real}}}{k_{\text{real}}} \times 100\% \tag{53}$$

Substituting Eqs. (51) and (52) into Eq. (53), we have:

$$\delta = \frac{b - a - ab}{a + b + ab} \epsilon \times 100\% \tag{54}$$

It is noted that the relative error δ is proportional to ϵ and is also affected by the volume ratios a and b . Generally, the difference between the mean pore pressure and equilibrium

Fig. 6 The error in permeability evaluation induced by choosing mean pore pressure as the characteristic pressure. Here, the upstream reservoir is assumed to have the same volume of the downstream one



pore pressure rises as ε increases, as does the error caused by the improper selection of characteristic pressure.

Figure 6 gives the variations of relative error δ with the volume ratio a and nonlinearity strength ε when two reservoirs of equal volume are used. Since the extra gas from upstream not only flows downstream but also fills the pores within the sample, the equilibrium pore pressure is always lower than the mean pore pressure, making the relative error δ negative. As the volume ratio of the pore to the reservoir tends to zero, the influence of pore filling becomes negligible, as well as the difference between the equilibrium pore pressure and the mean pore pressure, so that the relative error δ also tends to zero.

For the pulse-decay tests with constant pressure on one side, the expression for δ is:

$$\delta = \begin{cases} \varepsilon \times 100\%, & a = 0 \\ -\varepsilon \times 100\%, & b = 0 \end{cases} \quad (55)$$

which indicates that when the upstream or downstream pressure is kept constant, using mean pore pressure as the characteristic pressure can lead to an overestimation or underestimation of the apparent permeability, with the error expanding with the nonlinearity strength.

5.2 Effect of Nonlinearity on Duration

The pulse-decay test starts when a pressure pulse is applied and ends when the upstream and downstream pressure become equal. In general, the test duration becomes shorter when the sample has a larger cross-sectional area, a shorter length, and higher permeability (Jones 1997). To quantify the effect of nonlinearity on the duration, we assume that the core sample and experimental conditions remain the same and define that the pulse-decay tests terminate when the dimensionless pressure difference between the two ends of the sample decreases to 0.05, i.e.

$$\Delta P_D(\Gamma) = 0.05 \quad (56)$$

where Γ is the dimensionless duration of the test.

Take the logarithm of Eq. (52) and recall that $\ln \Delta P_D$ can be approximated as a linear function of time at the late-time stage of the pulse-decay test:

$$\ln \Delta P_D(\Gamma) = f - \theta_1^2 \Gamma = \ln(0.05) \quad (57)$$

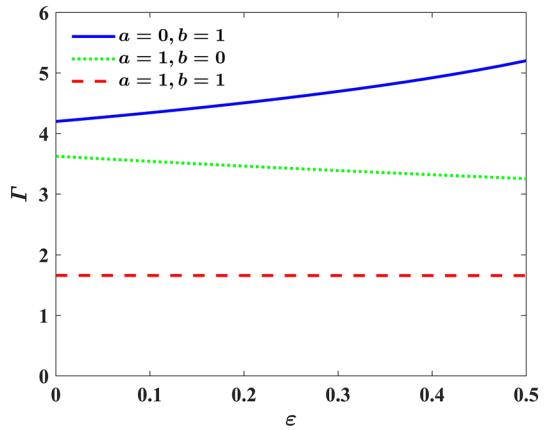
where f and $-\theta_1^2$ are the intercept and slope of the $\ln \Delta P_D$ vs. t_D plot, respectively.

By transforming Eq. (57), the expression for Γ can be obtained:

$$\Gamma = \frac{f - \ln(0.05)}{\theta_1^2} \quad (58)$$

It is noted that the θ_1^2 in the denominator is determined by Eq. (37) that only involves volume ratios a and b , and the constant $\ln(0.05)$ in the numerator just depends on the chosen end criterion. Equation (58) was first derived in Wang et al. (2021), where the initial differential pressure was assumed to be small to ensure the linearity of the governing equations. The present work considers pulse-decay tests with large initial differential pressure and therefore nonlinear governing equations. It is demonstrated that, similar to the linear cases, the pressure difference across the sample with nonlinear governing equations

Fig. 7 The variations of the duration of pulse-decay tests with nonlinearity strength



decays exponentially in the late-time stage, so Eq. (58) still applies. The nonlinearity only affects the intercept f , as seen in Fig. 4.

Previous studies have mainly focused on the effect of volume ratios on the time efficiency of the pulse-decay tests, and their results show that increasing the volume ratios (i.e., using smaller gas reservoirs) helps to increase θ_1^2 and, therefore, reduce the time cost (Jones 1997; Wang et al. 2021). Since we are concerned with the effect of nonlinearity on the duration, here the volume of the gas reservoirs is assumed to be equal to that of the core's pore space. Figure 7 presents the variations of the duration T with the nonlinearity strength ϵ , for the cases in which both ends of the sample are connected with a finite-volume reservoir ($a = b = 1$) or one end is kept at constant pressure ($a = 1, b = 0$ and $a = 0, b = 1$). It is noted that due to the larger volume ratio, the case ($a = b = 1$) always takes less time than the other two cases, which is consistent with the previous studies.

Since the nonlinearity speeds up the upstream pressure drop and slows down the downstream pressure increase, its final influence on the duration depends on the setup of the tests. For the symmetric case ($a = b = 1$), the effects of the nonlinearity on both sides largely cancel out, so the duration T remains almost constant, despite the nonlinearity strength ϵ . However, for the asymmetric cases that are affected by the nonlinearity only on one side, the duration T could increase ($a = 0, b = 1$) or decrease ($a = 1, b = 0$) with the nonlinearity strength ϵ . In practical measurements, the nonlinearity strength can be tuned by changing the initial pressure difference. Therefore, for pressure falloff measurements with a constant downstream pressure, increasing the initial pressure difference may help to reduce the time cost. In the original pulse-decay and pressure build-up cases, a small initial pressure difference is preferred.

6 Conclusions

Based on the law of conservation of mass and Darcy's law, the general nonlinear governing equation for the pulse-decay process is derived in this study, with the physical properties of the testing gas and the porous medium considered pressure-dependent. Through magnitude comparison, we found that for sedimentary matrix (shales, sandstones) samples tested by inert gases (He, Ar, N₂), only the pressure dependence of the gas compressibility and apparent permeability matters, yielding a simplified but still nonlinear governing equation.

The degree of the nonlinearity in the simplified equation is quantified by a dimensionless variable ε that is proportional to the initial pressure difference but inversely related to the characteristic pore pressure and slippage factor.

Through the perturbation method and the eigenfunction expansion method, the late-time behavior of the solution to the nonlinear governing equation is analyzed theoretically. The results show that the pressure difference between the two ends of the sample decays exponentially as time proceeds, and thus a straight line can be obtained at the late-time stage in the plot of logarithmic differential pressure versus time. The nonlinearity only affects the intercept of the line, not the slope, and apparent permeability can be evaluated from the latter, as long as the equilibrium pore pressure rather than the mean pore pressure is chosen as the characteristic pressure. The theoretical results were verified by numerical simulation. The simulation results further show that in the pulse-decay tests with the same core sample and equilibrium pore pressure but different initial pressure differences, the normalized upstream or downstream pressure transients will be separated from each other when the nonlinearity is considered, and it cannot be accounted for by the linear model. Such separation was observed in the experiments, which proves the importance of the nonlinear effect and the rationality of the proposed governing equation.

The error in the apparent permeability evaluation, which is induced by taking the mean pore pressure as the characteristic pressure, is discussed. The error increases linearly with the degree of nonlinearity and also depends on the volume ratios. For the pulse-decay tests with constant upstream (pressure build-up) or downstream pressure (pressure falloff), the permeability coefficients determined using this procedure will be overestimated or underestimated, respectively. The effect of nonlinearity on the duration of the pulse-decay test has also been investigated. It is found that for the tests with reservoirs of finite volume, the influence of nonlinearity on the upstream and downstream can be approximately offset. However, in the cases where the upstream or downstream pressure is maintained constant, the required duration of the tests will increase or decrease with the degree of nonlinearity, respectively. Notice that the assumptions of our model may be broken when the sample is highly stress-sensitive or the testing gas is absorptive (e.g., methane or carbon dioxide). Then the poroelasticity, adsorption, and real gas effects must be taken into account, which is the focus of our future studies.

Acknowledgements This work was financially supported by NSFC grants (No. U1837602, 11761131012) and the DFG grant AM 423/1-1 (Project number: 392108477; Joint Sino-German Research Project: “NanGasPor”).

Declarations

Conflict of interest The authors declare no conflict of interests.

References

- Abdelmalek, B., Karpyn, Z., Liu, S., Yoon, H., Dewers, T.: Gas permeability measurements from pressure pulse decay laboratory data using pseudo-pressure and pseudo-time transformations. *J. Pet. Explor. Prod. Technol.* **8**(3), 839–847 (2018)
- Akkutlu, I.Y., Fathi, E.: Multiscale gas transport in shales with local kerogen heterogeneities. *SPE J.* **17**(04), 1002–1011 (2012)
- Alnoaimi, K.R., Kovscek, A.R.: Influence of microcracks on flow and storage capacities of gas shales at core scale. *Transp. Porous Media* **127**(1), 53–84 (2019)

- Bender, C.M., Orszag, S.A.: Advanced mathematical methods for scientists and engineers I: asymptotic methods and perturbation theory. Springer Science & Business Media, Berlin (2013)
- Bhandari, A.R., Flemings, P.B., Polito, P.J., Cronin, M.B., Bryant, S.L.: Anisotropy and stress dependence of permeability in the Barnett shale. *Transp. Porous Media* **108**(2), 393–411 (2015)
- Boulin, P., Bretonnier, P., Gland, N., Lombard, J.-M.: Contribution of the steady state method to water permeability measurement in very low permeability porous media. *Oil Gas Sci. Technol.-Revue d'IFP Energ. Nouv* **67**(3), 387–401 (2012)
- Brace, W.F., Walsh, J., Frangos, W.: Permeability of granite under high pressure. *J. Geophys. Res.* **73**(6), 2225–2236 (1968)
- Callen, H.B.: Thermodynamics and an Introduction to Thermostatistics. Wiley, New York (1998)
- Chen, T., Feng, X.-T., Cui, G., Tan, Y., Pan, Z.: Experimental study of permeability change of organic-rich gas shales under high effective stress. *J. Nat. Gas Sci. Eng.* **64**, 1–14 (2019)
- Chenevert, M., Sharma, A.: Permeability and effective pore pressure of shales. *SPE Drill. Complet.* **8**(01), 28–34 (1993)
- Civan, F., Rai, C.S., Sondergeld, C.H.: Determining shale permeability to gas by simultaneous analysis of various pressure tests. *SPE J.* **17**(03), 717–726 (2012)
- Clarkson, C., Jensen, J., Chipperfield, S.: Unconventional gas reservoir evaluation: what do we have to consider? *J. Nat. Gas Sci. Eng.* **8**, 9–33 (2012)
- Crank, J., Nicolson, P.: A practical method for numerical evaluation of solutions of partial differential equations of the heat-conduction type. *Proc. Camb. Philos. Soc.* **43**(1), 50–67 (1947)
- Cui, X., Bustin, A., Bustin, R.M.: Measurements of gas permeability and diffusivity of tight reservoir rocks: different approaches and their applications. *Geofluids* **9**(3), 208–223 (2009)
- Darcy, H.: Les fontaines publiques de la ville de Dijon. Dalmont, Paris (1856)
- Davudov, D., Moghanloo, R.G., Lan, Y.: Evaluation of accessible porosity using mercury injection capillary pressure data in shale samples. *Energy Fuels* **32**(4), 4682–4694 (2018)
- Dicker, A.I., Smits, R.M.: A practical approach for determining permeability from laboratory pressure-pulse decay measurements. In: International Meeting on Petroleum Engineering. SPE 17578 (1988).
- Dong, J.-J., Hsu, J.-Y., Wu, W.-J., Shimamoto, T., Hung, J.-H., Yeh, E.-C., Wu, Y.-H., Sone, H.: Stress-dependence of the permeability and porosity of sandstone and shale from TCDP Hole-A. *Int. J. Rock Mech. Min. Sci.* **47**(7), 1141–1157 (2010)
- Fink, R., Krooss, B., Amann-Hildenbrand, A.: Stress-dependence of porosity and permeability of the Upper Jurassic Bossier shale: an experimental study. *Geol. Soc. Lond. Spec. Publ.* **454**(1), 107–130 (2017)
- Gaus, G., Amann-Hildenbrand, A., Krooss, B.M., Fink, R.: Gas permeability tests on core plugs from unconventional reservoir rocks under controlled stress: a comparison of different transient methods. *J. Nat. Gas Sci. Eng.* **65**, 224–236 (2019)
- Ghanizadeh, A., Amann-Hildenbrand, A., Gasparik, M., Gensterblum, Y., Krooss, B.M., Littke, R.: Experimental study of fluid transport processes in the matrix system of the European organic-rich shales: II. Posidonia Shale (Lower Toarcian, northern Germany). *Int. J. Coal Geol.* **123**, 20–33 (2014a)
- Ghanizadeh, A., Gasparik, M., Amann-Hildenbrand, A., Gensterblum, Y., Krooss, B.M.: Experimental study of fluid transport processes in the matrix system of the European organic-rich shales: I. Scandinavian Alum Shale. *Mar. Pet. Geol.* **51**, 79–99 (2014b)
- Hannon, M.J.: Alternative approaches for transient-flow laboratory-scale permeametry. *Transp. Porous Media* **114**(3), 719–746 (2016)
- Haskett, S.E., Narahara, G.M., Holditch, S.A.: A method for simultaneous determination of permeability and porosity in low-permeability cores. *SPE Form. Eval.* **3**(03), 651–658 (1988)
- Hatami, M., Bayless, D., Sarvestani, A.: Poroelastic effects on gas transport mechanisms and influence on apparent permeability in shale. *Int. J. Rock Mech. Min. Sci.* **153**, 105102 (2022)
- Heller, R., Vermynen, J., Zoback, M.: Experimental investigation of matrix permeability of gas shales. *AAPG Bull.* **98**(5), 975–995 (2014)
- Hinch, E.J.: Perturbation methods. In: Cambridge texts in applied mathematics. Cambridge University Press, Cambridge (1991)
- Hsieh, P.A., Tracy, J.V., Neuzil, C.E., Bredehoeft, J.D., Silliman, S.E.: A transient laboratory method for determining the hydraulic properties of 'tight' rocks—I, Theory. *Int. J. Rock Mech. Min. Sci. Geomech. Abstr.* **18**(3), 245–252 (1981)
- Jones, S.C.: A rapid accurate unsteady-state Klinkenberg permeameter. *Soc. Petrol. Eng. J.* **12**(05), 383–397 (1972)
- Jones, S.: A technique for faster pulse-decay permeability measurements in tight rocks. *SPE Form. Eval.* **12**(01), 19–26 (1997)
- Katsube, T.: Shale permeability and pore-structure evolution characteristics. Natural Resources Canada, Geological Survey of Canada, Ottawa (2000)

- Klinkenberg, L. J.: The permeability of porous media to liquids and gases, *API Drilling Prod. Pract.*, 200–213 (1941)
- Lasseux, D., Jannot, Y., Profice, S., Mallet, M.: The “Step Decay”: a new transient method for the simultaneous determination of intrinsic permeability, Klinkenberg coefficient and porosity on very tight rocks. In: *International Symposium of the Society of Core Analysts. SCA2012–25* (2012)
- Lemmon, E.W., McLinden, M.O., Friend, D.G.: Thermophysical properties of fluid systems. In: *Linstrom, P.J., Mallard, W.G. (eds.) NIST Chemistry WebBook, NIST Standard Reference Database Number 69. National Institute of Standards and Technology, Gaithersburg* (2023).
- Letham, E., Bustin, R.: Klinkenberg gas slippage measurements as a means for shale pore structure characterization. *Geofluids* **16**(2), 264–278 (2016)
- Liang, Y., Price, J.D., Wark, D.A., Watson, E.B.: Nonlinear pressure diffusion in a porous medium: approximate solutions with applications to permeability measurements using transient pulse decay method. *J. Geophys. Res. Solid Earth* **106**(B1), 529–535 (2001)
- Lin, Y.-Y., Myers, M.T.: Impact of non-linear transport properties on low permeability measurements. *J. Nat. Gas Sci. Eng.* **54**, 328–341 (2018)
- Lin, W.: Compressible fluid flow through rocks of variable permeability. In: *California Univ., Livermore (USA). Lawrence Livermore Lab.,* (1977)
- Liu, M.-M., Chen, Y.-F., Wei, K., Zhou, C.-B.: Interpretation of gas transient pulse tests on low-porosity rocks. *Geophys. J. Int.* **210**(3), 1845–1857 (2017)
- Loney, N.W.: *Applied mathematical methods for chemical engineers.* CRC Press, Boca Raton (2006)
- Lyu, Q., Shi, J., Gamage, R.P.: Effects of testing method, lithology and fluid-rock interactions on shale permeability: a review of laboratory measurements. *J. Nat. Gas Sci. Eng.* **78**, 103302 (2020)
- Ma, Y., Pan, Z., Zhong, N., Connell, L.D., Down, D.I., Lin, W., Zhang, Y.: Experimental study of anisotropic gas permeability and its relationship with fracture structure of Longmaxi Shales, Sichuan Basin, China. *Fuel* **180**, 106–115 (2016)
- Metwally, Y.M., Sondergeld, C.H.: Measuring low permeabilities of gas-sands and shales using a pressure transmission technique. *Int. J. Rock Mech. Min. Sci.* **48**(7), 1135–1144 (2011)
- Nolte, S., Fink, R., Krooss, B.M., Amann-Hildenbrand, A., Wang, Y., Wang, M., Schmatz, J., Klaver, J., Littke, R.: Experimental investigation of gas dynamic effects using nanoporous synthetic materials as tight rock analogues. *Transp. Porous Media* **137**(3), 519–553 (2021)
- Pan, Z., Ma, Y., Connell, L.D., Down, D.I., Camilleri, M.: Measuring anisotropic permeability using a cubic shale sample in a triaxial cell. *J. Nat. Gas Sci. Eng.* **26**, 336–344 (2015)
- Pang, Y., Soliman, M.Y., Deng, H., Emadi, H.: Analysis of effective porosity and effective permeability in shale-gas reservoirs with consideration of gas adsorption and stress effects. *SPE J.* **22**(06), 1739–1759 (2017)
- Richtmyer, R.D., Morton, K.W.: *Difference methods for initial-value problems.* Interscience Publishers, New York (1994)
- Riley, K.F., Hobson, M.P., Bence, S.J.: *Mathematical Methods for Physics and Engineering.* Cambridge University Press, Cambridge (1999)
- Rushing, J., Newsham, K., Lasswell, P., Cox, J., Blasingame, T.: Klinkenberg-corrected permeability measurements in tight gas sands: steady-state versus unsteady-state techniques. In: *SPE annual technical conference and exhibition. SPE 89867* (2004)
- Sander, R., Pan, Z., Connell, L.D.: Laboratory measurement of low permeability unconventional gas reservoir rocks: a review of experimental methods. *J. Nat. Gas Sci. Eng.* **37**, 248–279 (2017)
- Tinni, A., Fathi, E., Agarwal, R., Sondergeld, C.H., Akkutlu, I.Y., Rai, C.S.: Shale permeability measurements on plugs and crushed samples. In: *SPE canadian unconventional resources conference, SPE 162235* (2012)
- Trimmer, D.A.: Design criteria for laboratory measurements of low permeability rocks. *Geophys. Res. Lett.* **8**(9), 973–975 (1981)
- Walder, J., Nur, A.: Permeability measurement by the pulse-decay method: Effects of poroelastic phenomena and non-linear pore pressure diffusion. *Int. J. Rock Mech. Min. Sci. Geomech. Abstr.* **3**, 225–232 (1986)
- Wang, Y., Liu, S., Elsworth, D.: Laboratory investigations of gas flow behaviors in tight anthracite and evaluation of different pulse-decay methods on permeability estimation. *Int. J. Coal Geol.* **149**, 118–128 (2015)
- Wang, Y., Tian, Z., Nolte, S., Amann-Hildenbrand, A., Krooss, B.M., Wang, M.: Reassessment of transient permeability measurement for tight rocks: the role of boundary and initial conditions. *J. Nat. Gas Sci. Eng.* **95**, 104173 (2021)

- Wang, Y., Tian, Z., Nolte, S., Krooss, B.M., Wang, M.: An improved straight-line method for permeability and porosity determination for tight reservoirs using pulse-decay measurements. *J. Nat. Gas Sci. Eng.* **105**, 104708 (2022)
- Yang, Z., Sang, Q., Dong, M., Zhang, S., Li, Y., Gong, H.: A modified pressure-pulse decay method for determining permeabilities of tight reservoir cores. *J. Nat. Gas Sci. Eng.* **27**, 236–246 (2015).
- Zhang, R., Ning, Z., Yang, F., Wang, X., Zhao, H., Wang, Q.: Impacts of nanopore structure and elastic properties on stress-dependent permeability of gas shales. *J. Nat. Gas Sci. Eng.* **26**, 1663–1672 (2015)

Publisher's Note Springer Nature remains neutral with regard to jurisdictional claims in published maps and institutional affiliations.

Springer Nature or its licensor (e.g. a society or other partner) holds exclusive rights to this article under a publishing agreement with the author(s) or other rightsholder(s); author self-archiving of the accepted manuscript version of this article is solely governed by the terms of such publishing agreement and applicable law.